PhotoImmunoNanoTherapy Reveals an Anticancer Role for Sphingosine Kinase 2 and Dihydrosphingosine-1-Phosphate

Brian M. Barth,[†,‡,§,*] Sriram S. Shanmugavelandy,[†] James M. Kaiser,[†] Christopher McGovern,[⊥] Erhan İ. Altnoğlu,[∥] Jeremy K. Haakenson,[†] Jeremy A. Hengst,[†] Evan L. Gilius,[⊥] Sarah A. Knupp,[∥] Todd E. Fox,[†] Jill P. Smith,[⊥] Timothy M. Ritty,[¶] James H. Adair,[∥] and Mark Kester[†,§]

[†]Department of Pharmacology and [‡]Department of Medicine, Division of Hematology and Oncology, The Pennsylvania State University College of Medicine, Hershey, Pennsylvania 17033, United States, [§]Penn State Hershey Cancer Institute, Hershey, Pennsylvania 17033, United States, [⊥]Department of Medicine, Division of Gastroenterology, The Pennsylvania State University College of Medicine, Hershey, Pennsylvania 17033, United States, [∥]Department of Materials Science and Engineering, The Pennsylvania State University, University Park, Pennsylvania 16802, United States, and [¶]Department of Orthopaedics, The Pennsylvania State University College of Medicine, Hershey, Pennsylvania 17033, United States

ABSTRACT Tumor-associated inflammation mediates the development of a systemic immunosuppressive milieu that is a major obstacle to effective treatment of cancer. Inflammation has been shown to promote the systemic expansion of immature myeloid cells which have been shown to exert immunosuppressive activity in laboratory models of cancer as well as cancer patients. Consequentially, significant effort is underway toward the development of therapies that decrease tumor-associated inflammation and immunosuppressive cells. The current study demonstrated that a previously described deep tissue imaging modality, which utilized indocyanine green-loaded calcium phosphosilicate nanoparticles (ICG-CPSNPs), could be utilized as an immunoregulatory agent. The theranostic application of ICG-CPSNPs as photosensitizers for photodynamic therapy was shown to block tumor growth in murine models of breast cancer, pancreatic cancer, and metastatic osteosarcoma by decreasing inflammation-expanded immature myeloid cells. Therefore, this therapeutic modality was termed PhotoImmunoNanoTherapy. As phosphorylated sphingolipid metabolites have been shown to have immunomodulatory roles, it was hypothesized that the reduction of immature myeloid cells by PhotoImmunoNanoTherapy was dependent upon bioactive sphingolipids. Mechanistically, PhotoImmunoNanoTherapy induced a sphingosine kinase 2-dependent increase in sphingosine-1-phosphate and dihydrosphingosine-1-phosphate. Furthermore, dihydrosphingosine-1-phosphate was shown to selectively abrogate myeloid lineage cells while concomitantly allowing the expansion of lymphocytes that exerted an antitumor effect. Collectively, these findings revealed that PhotoImmunoNanoTherapy, utilizing the novel nontoxic theranostic agent ICG-CPSNP, can decrease tumor-associated inflammation and immature myeloid cells in a sphingosine kinase 2-dependent manner. These findings further defined a novel myeloid regulatory role for dihydrosphingosine-1-phosphate. PhotoImmunoNanoTherapy holds the potential to be a revolutionary treatment for cancers with inflammatory and immunosuppressive phenotypes.

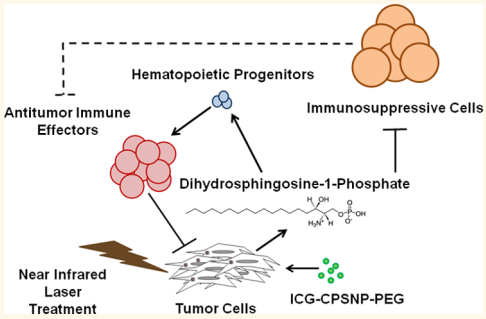

KEYWORDS: photodynamic therapy · calcium phosphosilicate nanoparticles · sphingosine kinase 2 · dihydrosphingosine-1-phosphate · tumor immunology

Photodynamic therapy (PDT) has emerged as an alternative strategy for the treatment of cancer. PDT takes advantage of an appropriate wavelength of light exciting a photosensitizer to an excited triplet energy state.[1,2] In the presence of molecular oxygen, which resides in a ground triplet state, energy is transferred to relax the excited state of the photosensitizer. This energy transfer in turn excites molecular oxygen to form excited singlet state oxygen ($^1O_2$). The effects of PDT have been attributed to $^1O_2$ triggering cell death *via* damaging oxidation or redox-sensitive cellular signaling pathways.[2,3] Unfortunately, PDT suffers from disadvantages associated with photosensitizer toxicity, a lack of efficacious and selective photosensitizers, as well as an inability of light to sufficiently penetrate through tissues to reach tumors deep within the body.[4,5]

Recently, we described the synthesis and utility of calcium phosphosilicate nanoparticles (CPSNPs).[6−13] In addition, we have published multiple reviews focused on the applications of

* Address correspondence to bmb14@psu.edu.

Received for review October 19, 2012 and accepted February 1, 2013.

Published online February 01, 2013
10.1021/nn304862b

CPSNPs.[14−18] CPSNPs are approximately 20 nm in diameter and offer an advantage over other nanoparticles because molecules of interest are encapsulated within the calcium phosphosilicate nanomatrix in contrast to surface decoration of the nanoparticle. Calcium and phosphate are advantageous materials for nanoparticles because they are abundant in physiological systems and pose no inherent toxicity. Additionally, the calcium phosphosilicate nanomatrix is stable at physiological pH, allowing these nanoparticles to protect their "payloads" during systemic circulation. CPSNPs are engulfed by cells during endocytosis and ultimately trafficked *via* the endosomal−lysosomal pathway where acidic pH changes cause the CPSNPs to degrade and release their contents. More specifically, CPSNPs were shown to increase the quantum efficiency and photostability of encapsulated fluorescent dyes, while surface functionalization with polyethylene glycol (PEG) further allowed for efficient *in vivo* imaging using indocyanine green (ICG)-loaded CPSNPs *via* enhanced permeation and retention of the particles within xenografted breast and pancreatic cancer tumors.[8,9] ICG is a near-infrared (NIR) fluorescing dye that has been approved by the Food and Drug Administration of the United States of America for use in medical imaging. Unfortunately, use of ICG is limited by its short plasma half-life (2−4 min), photobleaching, and nonspecific quenching due to binding with serum proteins.[19] Encapsulation within CPSNPs enhanced the fluorescence quantum efficiency (Φ_F) and photostability of ICG.[8,12] With approximately 6 ± 2 ICG molecules encapsulated per typical CPSNP, the Φ_F of the individual encapsulated molecules increased to 0.053 ± 0.003 compared with 0.027 ± 0.001 for free ICG molecules.[12] The utility of ICG encapsulated within CPSNPs for deep tissue imaging is also related to the ability of longer wavelength NIR light to penetrate through tissue.[8,9] Surface targeting moieties were successfully coupled to CPSNPs, which allowed for specific targeting to breast or pancreatic cancer tumors to improve diagnostic imaging.[9] Recently, successful targeting of ICG-loaded CPSNPs to leukemia stem cells allowed for successful *in vivo* PDT of chronic myeloid leukemia and myelomonocytic leukemia.[11,14] Owing in part to the low toxicity of CPSNPs, minimal myelosuppression was observed despite the robust antileukemic effect of PDT using ICG-loaded CPSNPs.[11]

Many chemotherapeutics, radiation therapy, and PDT have been shown to increase levels of the sphingolipid ceramide in cancerous tissue, while relapsing and therapy-resistant cancers possess the inherent ability to detoxify ceramide to pro-oncogenic neutral or phosphorylated metabolites.[20−24] Sphingolipids are an extensive classification of lipids which play prominent roles in cellular signaling. The most well-studied sphingolipid is ceramide, an N-acylated sphingosine, which serves as a hypothetical center of sphingolipid metabolism.[24,25] Ceramide is synthesized *de novo* from the condensation of serine with the saturated C16:0 fatty acid palmitic acid, is converted to a diversity of complex sphingolipids *via* headgroup addition, and is resynthesized *via* the breakdown of complex sphingolipids. The conversion of ceramide to sphingosine-1-phosphate (S1P) has been extensively studied, namely, due to ceramide's role as a pro-apoptotic, pro-cellular stress, anti-inflammatory lipid and S1P's role as a pro-survival, mitogenic, and oncogenic lipid.[24,26] Importantly, S1P has also been shown to be immunogenic, stimulating cells of the immune system and promoting their trafficking, *via* binding to S1P G-protein-coupled receptors.[26−29]

Recently, immune-suppressive cells have gained notoriety as critical cellular regulators by which tumors evade immunity and overcome therapeutic intervention. These suppressive cells include a heterogeneous population of immature myeloid cells expanded systemically as a consequence of a profound tumor-associated pro-inflammatory milieu, likely prematurely mobilized myeloid progenitors, and which have also been referred to as myeloid-derived suppressor cells (MDSCs).[30−34] Anticancer T-cell-dependent and -independent immune responses have been shown to be negatively regulated by MDSCs in a diversity of models of cancer.[30,31] In addition to tumors, MDSCs are found at high numbers in the peripheral circulation and in organs such as the spleen and liver, and their systemic numbers are directly correlated with tumor burden.[30,31] These immunosuppressive myeloid cells have been identified in both humans and mice, including athymic nude mice, with populations defined by the presence of particular combinations of surface antigens. In mice, MDSCs are reported to be Gr-1+ CD11b+ granulocytic or monocytic cells, while in humans they are primarily defined within a CD14- HLA-DR- CD33+ CD11b+ population.[30,31,35] There is debate between the definition of MDSC and all immature myeloid cells, as MDSC specifically implies that immunosuppressive activity has been measured. In this study, we will subsequently refer to this population as immature myeloid cells because we have characterized them solely based on coexpression of the surface markers Gr-1 and CD11b.

In this study, PDT utilizing ICG-CPSNPs was evaluated in murine models of breast cancer, pancreatic cancer, and metastatic osteosarcoma. It was hypothesized that PDT utilizing ICG-CPSNPs could be employed as a "theranostic" modality for solid tumors and that its efficacy would be due in part to regulation of the immune milieu (referred to hereafter as PhotoImmunoNanoTherapy). Indeed, a robust antitumor response was observed and was linked to a reduction of tumor-associated inflammation and immature myeloid cells. Moreover, the therapeutic efficacy of PhotoImmunoNanoTherapy was revealed to be dependent on sphingosine kinase 2 rather than ceramide-generating pathways more commonly associated with anticancer therapies.

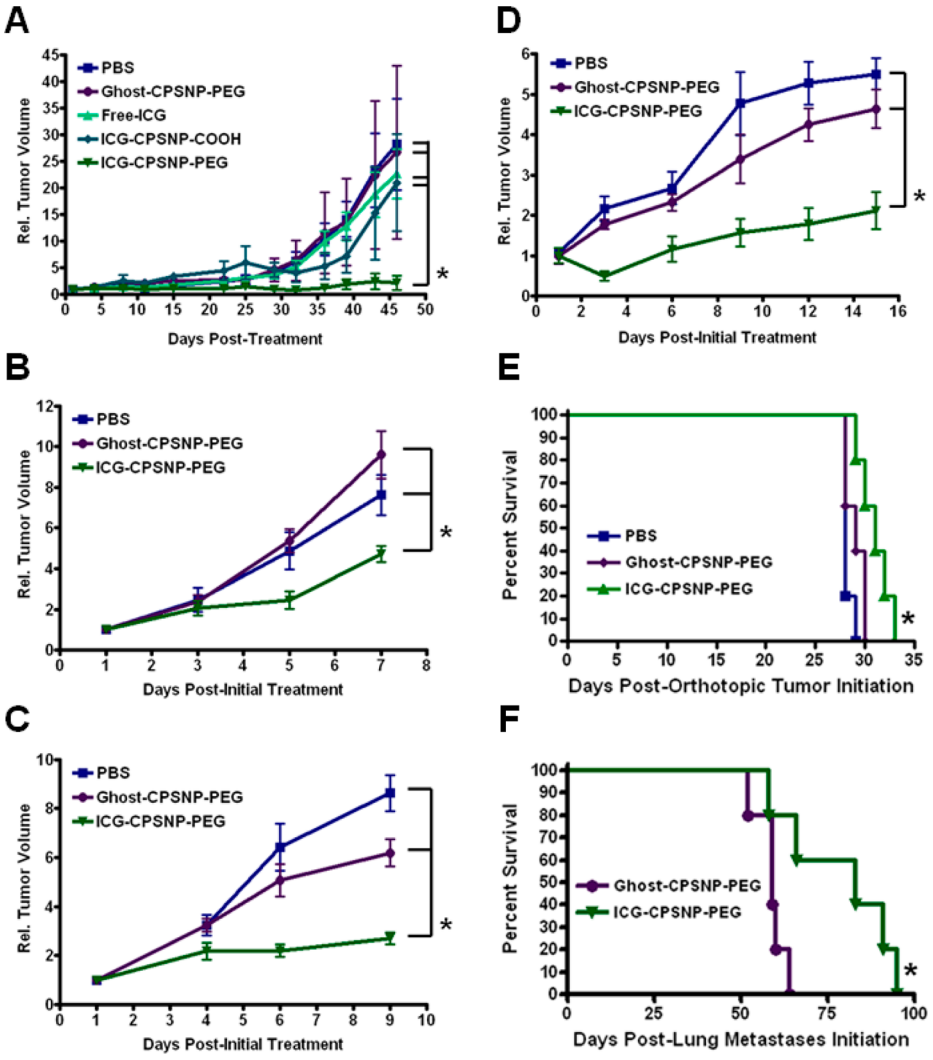

Figure 1. PhotoImmunoNanoTherapy decreases tumor burden and improves survival (ICG, indocyanine green; ghost, empty; CPSNP, calcium phosphosilicate nanoparticles; COOH, citrate-functionalized; PEG, PEGylated). (A) Tumor growth following PhotoImmunoNanoTherapy was monitored in athymic nude mice engrafted with human MDA-MB-231 breast cancer cells. ANOVA, *$p < 0.05$ compared to all, $n \geq 5$. (B) Tumor growth following PhotoImmunoNanoTherapy was monitored in BALB/cJ mice engrafted with murine 410.4 breast cancer cells. ANOVA, *$p < 0.05$ compared to all, $n \geq 8$. (C) Tumor growth following PhotoImmunoNanoTherapy was monitored in NOD.CB17-*Prkdc*^{scid}/J mice engrafted with murine 410.4 breast cancer cells. ANOVA, *$p < 0.001$ compared to all, $n \geq 7$. (D) Tumor growth following PhotoImmunoNanoTherapy was monitored in C57BL/6J mice engrafted with murine Panc-02 pancreatic cancer cells. ANOVA, *$p < 0.05$ compared to all, $n \geq 6$. (E) Survival of athymic nude mice orthotopically implanted with human BxPC-3-GFP pancreatic cancer cells was monitored following PhotoImmunoNanoTherapy. Logrank test, *$p < 0.05$ compared to all, $n = 5$. (F) Survival of athymic nude mice with experimental lung metastases of human SAOS-2-LM7 osteosarcoma cells was monitored following PhotoImmunoNanoTherapy. Logrank test, *$p < 0.05$, $n = 5$.

RESULTS AND DISCUSSION

PhotoImmunoNanoTherapy Blocks Tumor Progression and Extends Survival. The development of more efficacious and less toxic cancer therapies is a priority due to the prevalence and poor prognosis of the disease. Current cancer therapies are highly toxic and offer a range of potential efficacy that varies with the subtype and staging of the disease. PDT has emerged as an alternative to traditional chemotherapy and radiation therapy for the treatment of certain types of cancer but not breast or pancreatic cancer or metastatic osteosarcoma.[1,2] The efficacy of conventional PDT is limited by photosensitizers that offer limited optical characteristics and high toxicity.[4,5] For these reasons, PDT is currently limited primarily to the treatment of cancers of the skin and esophagus.[2,36,37] The development and utilization of ICG-CPSNPs initially was postulated to improve diagnostic imaging for breast cancer.[8,9] Intriguingly, this advancement in imaging with ICG-CPSNPs also overcame limitations associated with traditional PDT.[8,11,14] Upon the basis of the improved quantum efficiency and improved half-life, it was hypothesized that ICG-CPSNPs could be used as a theranostic modality for cancer. Importantly, ICG-CPSNPs have been shown to be relatively nontoxic during PDT of leukemia as evidenced by limited myelosuppression,[11,14] as well as a lack of a change in body weight during therapy (Supporting Information Figure S1).

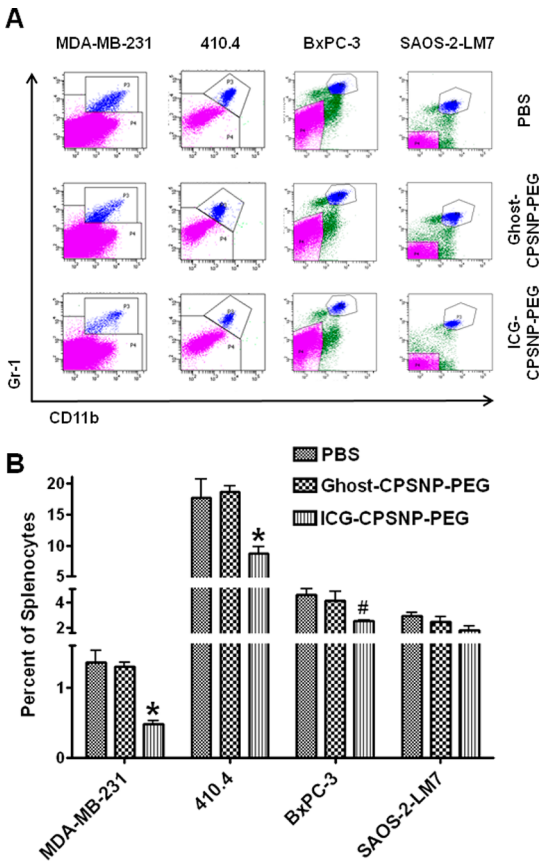

Figure 2. PhotoImmunoNanoTherapy diminishes the immature myeloid immune milieu. Splenic immature myeloid cells (Gr-1+ CD11b+) were decreased five days following PhotoImmunoNanoTherapy of various cancer models. (A) Representative dot plots from athymic nude mice with MDA-MB-231 breast cancer tumors, BALB/cJ mice with 410.4 breast cancer tumors, athymic nude mice with orthotopic BxPC-3 pancreatic cancer tumors, or athymic nude mice with SAOS-2-LM7 experimental lung metastasis of osteosarcoma. (B) Percent of immature myeloid cells determined by flow cytometry of splenocytes. ANOVA, *$p < 0.05$ compared to all, $^{\#}p = 0.05$ compared to all, $n \geq 4$.

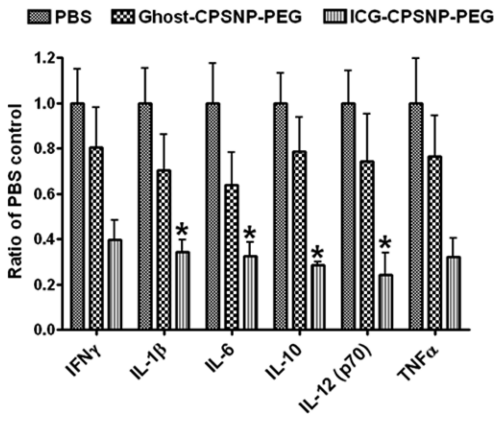

Figure 3. PhotoImmunoNanoTherapy diminishes the systemic inflammatory milieu. Serum collected from MDA-MB-231 tumor-bearing athymic nude mice one day following PhotoImmunoNanoTherapy was collected, and a cytokine multiplex assay was used to quantify IL-1β, IL-6, IL-12(p70), IL-10, IFNγ, and TNFα. ANOVA, *$p < 0.05$ compared to all, $n = 3$.

To evaluate the antitumor efficacy of PhotoImmunoNanoTherapy, two murine models of breast cancer were utilized to study effects in T-cell-competent hosts (murine 410.4 cells in BALB/cJ mice) and T-cell-deficient hosts (human MDA-MB-231 cells in athymic nude mice; murine 410.4 cells in NOD.CB17-*Prkdc*^{scid}/J mice), in addition to a subcutaneously engrafted model of pancreatic cancer (murine Panc-02 cells in C57BL/6J mice), an orthotopic pancreatic cancer model (human BxPC-3 cells in athymic nude mice), and an experimental model of lung-metastatic osteosarcoma (human SAOS-2-LM7 cells in athymic nude mice). Treatments were initiated one week following tumor establishment and consisted of injections of ICG-CPSNPs or controls followed 24 h later by NIR laser treatment of the tumor location to allow adequate tumor accumulation of PEGylated ICG-CPSNPs. Tumor growth was effectively blocked and survival extended by PhotoImmunoNanoTherapy in (Figure 1A–F): (1) human MDA-MB-231 cells in athymic nude mice (subcutaneous), (2) murine 410.4 breast cancer cells in BALB/cJ mice (subcutaneous), (3) murine 410.4 breast cancer cells in NOD.CB17-*Prkdc*^{scid}/J mice (subcutaneous), (4) murine Panc-02 pancreatic cancer cells in C57BL/6J mice (subcutaneous), (5) human BxPC-3-GFP pancreatic cancer cells in athymic nude mice (orthotopic), and (6) human SAOS-2-LM7 osteosarcoma cells in athymic nude mice (experimental lung metastases). In the most elaborate study, MDA-MB-231 tumor growth was abrogated in athymic nude mice receiving PEGylated ICG-CPSNPs but not PBS or PEGylated ghost CPSNPs (Figure 1A). Furthermore, MDA-MB-231 tumor growth was not blocked by non-PEGylated (citrate-terminated) ICG-CPSNPs or free ICG. This observation is consistent with previous findings which demonstrated that only PEGylated ICG-CPSNPs, but not non-PEGylated ICG-CPSNPs or free ICG, accumulated within MDA-MB-231 tumors,[8,9] indicating that the presence of ICG-CPSNPs within tumors is required for antitumor efficacy of PhotoImmunoNanoTherapy. Long-term blockade of tumor growth with a minimal treatment suggested a possible antitumor immune response, while the efficacy in athymic nude mice and NOD.CB17-*Prkdc*^{scid}/J mice further suggested a T-cell-independent and B-cell-independent antitumor response.

Inflammation-Expanded Immature Myeloid Cells Are Decreased by PhotoImmunoNanoTherapy. Anticancer T-cell-dependent and -independent immune responses have previously been shown to be negatively regulated by immature myeloid cells.[30,31] To evaluate regulation of immature myeloid cells by PhotoImmunoNanoTherapy, MDA-MB-231 or 410.4 tumor-bearing BALB/cJ mice were sacrificed five days post-NIR laser treatment. All models of tumor-bearing mice contained splenocyte populations of Gr-1+ CD11b+ immature myeloid cells (Figure 2A). The immature myeloid cells of MDA-MB-231 tumor-bearing athymic nude mice also stained positive for the gp91^{phox} subunit of the NADPH oxidase, an enzyme critical to their immunosuppressive nature of

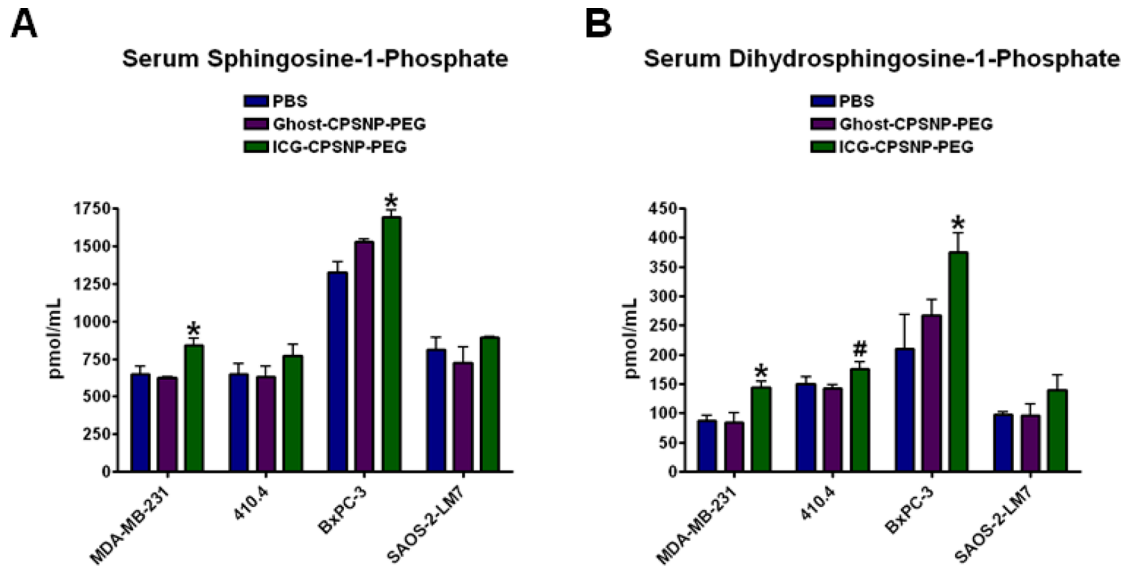

Figure 4. PhotoImmunoNanoTherapy increases the serum levels of phosphorylated bioactive sphingolipids. (A) S1P (ANOVA, *$p < 0.05$ compared to all) and (B) dhS1P (ANOVA, *$p < 0.05$ compared to all, unpaired student's t test, $^{\#}p < 0.05$ compared to ghost CPSNP-PEG only, $n \geq 3$) were quantified by LC-MS^3 in the serum of human MDA-MB-231 subcutaneous breast cancer tumor-bearing athymic nude mice, murine 410.4 subcutaneous breast cancer tumor-bearing BALB/cJ mice, human BxPC-3-GFP orthotopic pancreatic cancer tumor-bearing athymic nude mice, and human SAOS-2-LM7 experimental lung-metastatic osteosarcoma tumor-bearing athymic nude mice five days following treatment with PhotoImmunoNanoTherapy.

MDSCs,[30,31] and were also predominately CD44+ and CD115+, both markers that have been associated with MDSCs (Supporting Information Figure S2A). The Gr-1+ surface antigen on this immature myeloid cell population in MDA-MB-231 tumor-bearing mice was mostly LY-6G+ (88%), as opposed to LY-6C (12%), which indicates that this cell population is of a more granulocytic nature (Supporting Information Figure S2B). Additionally, the immature myeloid cells generated reactive oxygen species (ROS) in response to stimulation with phorbol-12-myristate-13-acetate (Supporting Information Figure S2C), a trait that has been associated with the immunosuppressive nature of these cells.[32] PhotoImmunoNanoTherapy caused a significant decrease in splenic Gr-1+ CD11b+ immature myeloid cells, in MDA-MB-231 tumor-bearing athymic nude mice, whereas treatment with PBS or PEGylated ghost CPSNPs did not (Figure 2). This PhotoImmunoNanoTherapy-induced decrease in splenic immature myeloid cells was also observed in 410.4 tumor-bearing BALB/cJ mice (Figure 2). In a similar manner, PhotoImmunoNanoTherapy caused a significant decrease in splenic immature myeloid cells in BxPC-3 orthotopic pancreatic tumor-bearing athymic nude mice and a modest decrease in athymic nude mice bearing SAOS-2-LM7 experimental lung metastases (Figure 2).

An important aspect of immature myeloid cells, or MDSC, biology is the profound inflammatory milieu which they develop and thrive in.[30,31] In this study, serum was collected from MDA-MB-231 tumor-bearing athymic nude mice 24 h following NIR treatment, and a cytokine multiplex assay was performed. PhotoImmunoNanoTherapy, but not controls, significantly decreased the levels of IL-1β, IL-6, IL-12, and IL-10 and also appeared to reduce the levels of IFNγ and TNFα although not significantly (Figure 3). Combined, these results showed that PhotoImmunoNanoTherapy decreased immature myeloid cells and the inflammatory milieu critical to their expansion during tumor progression.

PhotoImmunoNanoTherapy Triggers an Increase of Phosphorylated Bioactive Sphingolipids. To explore how PhotoImmunoNanoTherapy could be regulating the immune system, an analysis of the "sphingolipidome" was studied in tumors and serum collected from treated tumor-bearing mice. As PhotoImmunoNanoTherapy modulated the immune system and was efficacious in both athymic nude mice and BALB/cJ mice, in depth "sphingolipidomic" studies were performed in athymic nude mice bearing MDA-MB-231 tumors to focus more precisely on mediation of T-cell-independent immunity as well as BALB/cJ mice bearing 410.4 tumors (Supporting Information Figure S3A−F; Figure 4A,B). Tumor sphingolipidomic studies revealed that ceramides were mostly unchanged with the exception of a minor increase in C24:1 in BALB/cJ mice (410.4 tumors) (Supporting Information Figure S3B). Intriguingly, an increase in tumor S1P was observed as a function of PhotoImmunoNanoTherapy in both models (Supporting Information Figure S3D), as well as an increase in the precursor sphingosine in the athymic nude mouse model (MDA-MB-231 tumor) (Supporting Information Figure S3C). In contrast, a sphingolipidomic analysis of the serum of treated mice revealed that both S1P and its related bioactive sphingolipid dihydrosphingosine-1-phosphate (dhS1P) were significantly elevated in the serum of PhotoImmunoNanoTherapy-treated athymic nude mice with subcutaneous MDA-MB-231 tumors or with orthotopic BxPC-3 tumors (Figure 4A,B). Modest

A

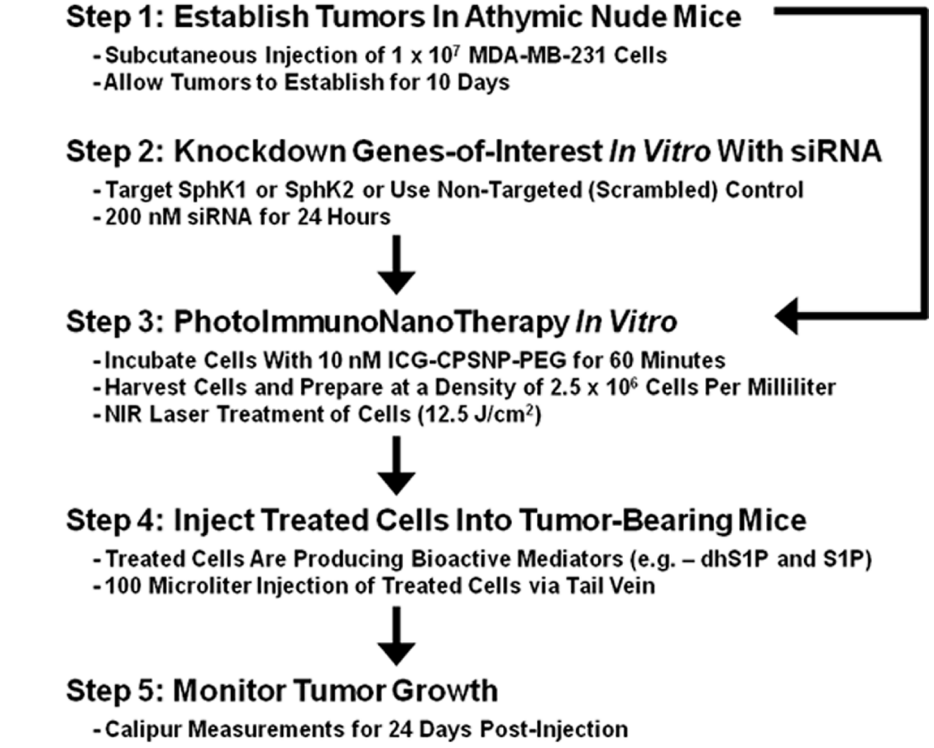

B

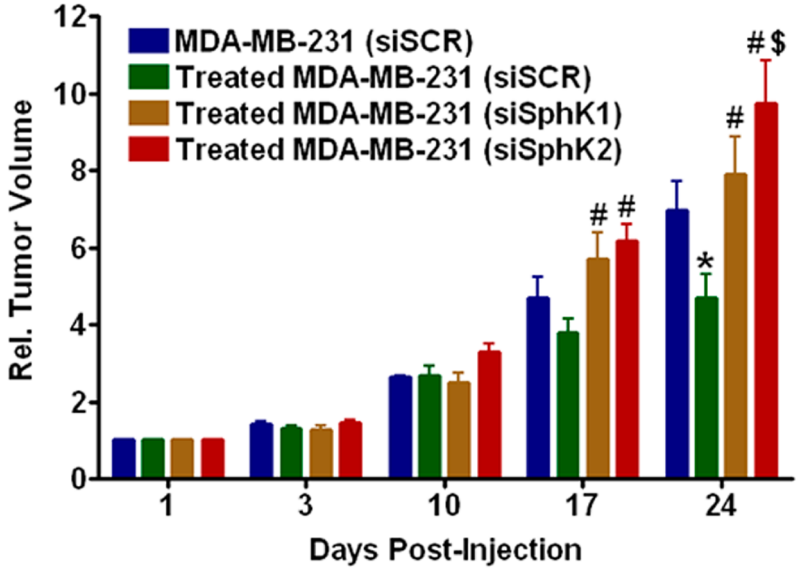

Figure 5. Therapeutic efficacy of PhotoImmunoNanoTherapy requires a sphingosine kinase. (A) Schematic depicting the experimental model where cancer cells treated in culture with PhotoImmunoNanoTherapy are harvested and then injected systemically into tumor-bearing mice. The premise was that treatment would trigger the release of sphingosine-1-phosphate (S1P) and dihydrosphingosine-1-phosphate (dhS1P) and that one of these or both would exert an antitumor effect. This strategy allowed interference with S1P/dhS1P-producing sphingosine kinases (SphKs) with siRNA in the cultured cancer cells. (B) Cultured MDA-MB-231 cells, first exposed to siRNA (siSCR, scrambled control siRNA; siSK1, SphK1 siRNA; siSK2, SphK2 siRNA), were treated in culture with PhotoImmunoNanoTherapy according to the schematic depicted in panel A and then injected into MDA-MB-231 tumor-bearing athymic nude mice. Alternatively, MDA-MB-231 cells exposed only to scrambled control siRNA without any near-infrared (NIR) light treatment were injected as controls. ANOVA, $^{*}p < 0.05$ compared to all, $^{\#}p < 0.05$ compared to PBS, untreated cells exposed to scrambled control siRNA, $^{\$}p < 0.05$ compared to NIR-treated cells exposed to SphK1 siRNA, $n \geq 5$.

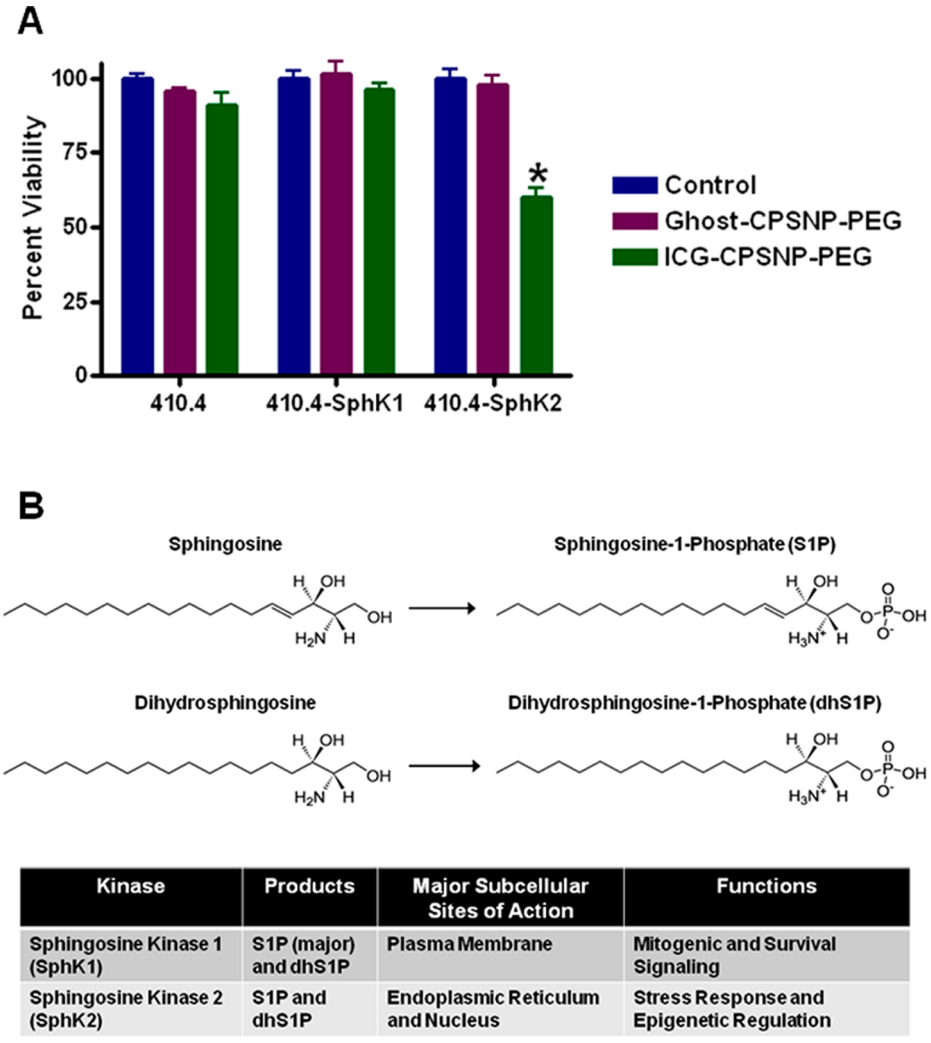

Kinase	Products	Major Subcellular Sites of Action	Functions
Sphingosine Kinase 1 (SphK1)	S1P (major) and dhS1P	Plasma Membrane	Mitogenic and Survival Signaling
Sphingosine Kinase 2 (SphK2)	S1P and dhS1P	Endoplasmic Reticulum and Nucleus	Stress Response and Epigenetic Regulation

Figure 6. Sphingosine kinase 2 mediates the therapeutic efficacy of PhotoImmunoNanoTherapy. (A) 410.4 cells stably expressing either SphK1 or SphK2 were exposed to normally nontoxic PhotoImmunoNanoTherapy conditions (10 nM ICG-CPSNP-PEG and 0.2 J/cm^2 NIR irradiation), and cellular viability was evaluated. ANOVA, *$p < 0.05$ compared to all, $n = 4$. (B) Chemical structures of sphingosine, dihydrosphingosine, sphingosine-1-phosphate (S1P), and dihydrosphingosine-1-phosphate (dhS1P), as well as a short table describing the products, major subcellular sites of action, and known functions of sphingosine kinases (SphKs).

elevations of serum dhS1P were also observed in the serum of PhotoImmunoNanoTherapy-treated BALB/cJ mice bearing 410.4 tumors (Figure 4B). Of particular interest, the mass levels of phosphorylated sphingolipid species were much higher in serum than in tumor tissue possibly reflective of a release of phosphorylated sphingolipids in response to PhotoImmunoNanoTherapy. Intriguingly, the increase in the amount of dhS1P was more dramatic than the increase in S1P. In the MDA-MB-231, BxPC-3, and SAOS-2-LM7 models, there were a 65, 79, and 43% increase in dhS1P, respectively, and these compared with respective increases in S1P of only 29, 27, and 10%. These data suggest that PhotoImmunoNanoTherapy initiates specific alterations of the sphingolipidome, possibly resulting in the production and release of bioactive phosphorylated sphingolipid metabolites into systemic circulation. Like S1P, dhS1P is generated by sphingosine kinase (SphK) activity, but unlike S1P, no significant role has been attributed to dhS1P.[24,26] Much attention has been given to the role of ceramides in the induction of cell death and, in particular, in response to chemotherapy, radiation therapy, and even PDT.[20−24] In cancer, sphingolipids such as S1P are often elevated, while ceramides are decreased, providing an environment friendly to tumor growth.[21−24,38] Therefore, the specific increase in S1P and dhS1P observed in response to PhotoImmunoNanoTherapy was particularly intriguing and thought to mediate a potentially novel antitumor mechanism.

Sphingosine Linase 2 Mediates the Antitumor Effects of PhotoImmunoNanoTherapy. To confirm a potentially novel role for SphKs and S1P and/or dhS1P in modulating the antitumor effect of PhotoImmunoNanoTherapy, an experimental model was developed where MDA-MB-231 cells were treated in culture with PhotoImmunoNanoTherapy and then injected systemically into tumor-bearing mice (Figure 5A). The premise was that

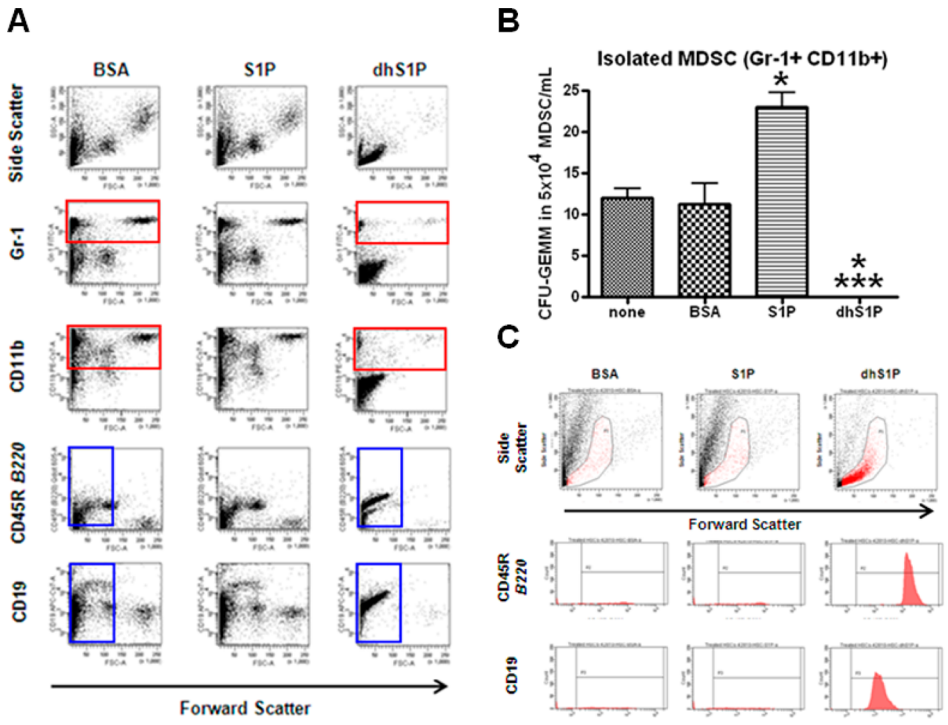

Figure 7. Isolated immature myeloid cells from tumor-bearing athymic nude mice are decreased by dhS1P treatment while cells with B-cell characteristics are expanded from hematopoietic progenitors. (A) Splenic immature myeloid cells (Gr-1+ CD11b+, also defined as MDSCs: myeloid-derived suppressor cells) were isolated from MDA-MB-231 tumor-bearing athymic nude mice and exposed to BSA, S1P (5 μM), or dhS1P (5 μM). Following 24 h culture incubation, cells were labeled with specific antibodies and analyzed by multicolor flow cytometry (red, immature myeloid cells; blue, probable B-cells). (B) Splenic immature myeloid cells were isolated from MDA-MB-231 tumor-bearing athymic nude mice and cultured (5×10^4 cells/mL) in GEMM-supportive semisolid media with BSA, S1P (5 μM), or dhS1P (5 μM). GEMM colonies (multipotent myeloid progenitor cells) were visualized and counted after 3 weeks of culture. ANOVA, *$p < 0.01$ compared to no treatment or BSA-treatment, ***$p < 0.001$ compared to S1P-treatment, $n \geq 3$. (C) Splenic hematopoietic progenitors (lineage-Sca-1+ CD117+) were isolated from MDA-MB-231 tumor-bearing athymic nude mice and exposed to BSA, S1P (5 μM), or dhS1P (5 μM). Following 24 h culture incubation, cells were labeled with specific antibodies and analyzed by multicolor flow cytometry.

the PhotoImmunoNanoTherapy treatment would trigger the release of S1P, dhS1P, or other S1P/dhS1P-regulated bioactive mediators, and that this would exert an antitumor effect. Indeed, this experimental strategy blocked tumor growth, while abrogation of SphK1 or SphK2 with siRNA completely eliminated any antitumor effect (Figure 5B). These findings demonstrated that lipids generated by SphKs in cancer cells mediate the antitumor effect of PhotoImmunoNanoTherapy because knockout of SphKs abrogated the therapeutic effect.

To further verify the role of SphKs, a contrasting strategy was employed where overexpression of SphKs was used to promote the PhotoImmunoNanoTherapy effect. First, 410.4 cells stably expressing either SphK1 or SphK2 were exposed to PhotoImmunoNanoTherapy conditions that otherwise would not result in any therapeutic effect (10 nM ICG-CPSNP-PEG and 0.2 J/cm^2 NIR irradiation). Only SphK2 overexpression resulted in sensitivity to PhotoImmunoNanoTherapy under these conditions (Figure 6A), further implicating SphK2 as the key regulator of PhotoImmunoNanoTherapy. Intriguingly, it has been reported that S1P generated in the nucleus by SphK2 is implicated in epigenetic regulation,[39] and it is possible that multiple phosphorylated lipid-signaling molecules mediate the efficacy of PhotoImmunoNanoTherapy through effects at surface receptors or as epigenetic regulators.[24,26,39] Indeed, nuclear production of S1P by SphK2 was recently shown to mediate epigenetic regulation of genes governing cellular stress.[39] The chemical structures of the substrates and products of SphK activity, as well as a brief table depicting the major subcellular sites of action and known functions of SphKs, are given (Figure 6B). In the present study, SphK2 was shown to mediate the efficacy of PhotoImmunoNanoTherapy perhaps due to epigenetic regulation of an anti-inflammatory program that may subsequently be responsible for the observed decrease in tumor-associated inflammation and immature myeloid cells. It is also noteworthy that the study evaluating the epigenetic role for S1P in the nucleus also detected dhS1P and never distinguished a specific role for either lipid.[39] Moreover, the diverse membrane localization of SphK2 puts it in an optimal subcellular position to generate dhS1P at membranes that are rich in dihydrosphingosine, such as the endoplasmic reticulum.

Dihydrosphingosine-1-Phosphate Abrogates the Propagation of Tumor-Amplified Immature Myeloid Cells That Allows Concomitant Expansion of Antitumor Lymphocytes. The final aspect of

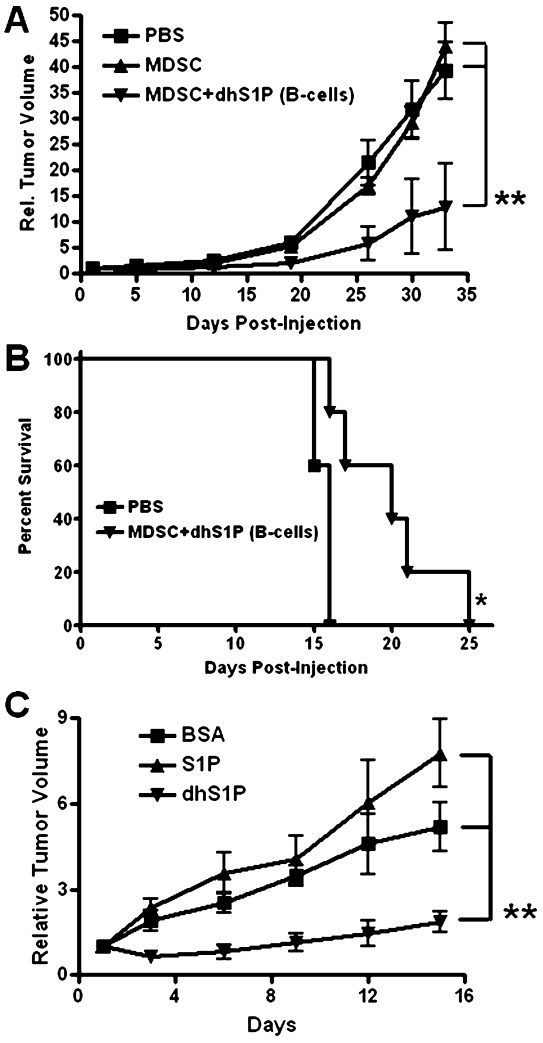

Figure 8. Dihydrosphingosine-1-phosphate (dhS1P) exerts specific antitumor roles. (A) Splenic immature myeloid cells (Gr-1+ CD11b+, also defined as MDSC: myeloid-derived suppressor cells) were isolated from subcutaneous human MDA-MB-231 breast tumor-bearing athymic nude mice, treated with or without dhS1P (to induce the expansion of CD19+ CD45R *B220*+ cells: B-cells), and adoptively transferred into subcutaneous human MDA-MB-231 breast tumor-bearing athymic nude mice before monitoring tumor growth. ANOVA, $^{**}p < 0.05$ compared to PBS control, $n \geq 6$. (B) Splenic immature myeloid cells were isolated from orthotopic human BxPC-3 pancreatic tumor-bearing athymic nude mice, treated with or without dhS1P, and adoptively transferred into orthotopic human BxPC-3 pancreatic tumor-bearing athymic nude mice before monitoring survival. Logrank test, $^{*}p < 0.05$, $n = 5$. (C) Tumor growth following BSA (lipid carrier control), sphingosine-1-phosphate (S1P), or dhS1P injection every other day was monitored in C57BL/6J mice engrafted with subcutaneous murine Panc-02 pancreatic cancer cells. ANOVA, $^{**}p < 0.05$ compared to BSA control, $n \geq 6$.

our study more closely evaluated the effects of dhS1P at the level of hematopoietic cells. Specifically, the effects of dhS1P were directly compared with those of S1P as to delineate a difference in their physiological roles. Tumor-expanded immature myeloid cells were isolated and exposed in culture to either dhS1P or S1P. Given the robust increase in dhS1P compared with S1P that was observed in response to PhotoImmunoNanoTherapy in the *in vivo* studies, it was of little surprise that only dhS1P exerted an effect on isolated immature myeloid cells in culture. Specifically, multicolor flow cytometry revealed that cells bearing the surface characteristics of immature myeloid cells were completely ablated under normal culture conditions by dhS1P treatment but not S1P treatment (Figure 7A). This was confirmed by repeating the same dhS1P, or S1P, treatments on isolated immature myeloid cells but in growth-factor-supplemented media as a colony-forming assay. Isolated immature myeloid cells were cultured in CFU (colony-forming unit)-GEMM (granulocyte, erythrocyte, monocyte, megakaryocyte) supportive semisolid media and formed GEMM colonies indicative of their multipotent myeloid progenitor nature (Figure 7B). This specific colony growth was shown to be dramatically augmented by S1P treatment. In contrast, CFU-GEMM colony formation was completely abrogated by exposure to dhS1P, indicative of the lipid's potent regulatory effect. Intriguingly, dhS1P exposure also promoted the expansion of a new population of cells in culture which displayed CD19 and CD45R *B220* on their surface—markers that are indicative of B-cells (Figure 7A). Importantly, we observed this same expansion of CD19+ CD45R *B220*+ cells within splenocyte isolations from tumor-bearing mice treated with PhotoImmunoNanoTherapy (Supporting Information Figure S4). In addition, PhotoImmunoNanoTherapy triggered the expansion of cells bearing the expression of the natural killer (NK) cell marker CD49b *DX5*—a lymphocyte population known for antitumor activity (Supporting Information Figure S5). It is possible that these effects are indirect, in that dhS1P-mediated suppression of immature myeloid cells simply removes a blockade of lymphoid differentiation. In agreement with this idea, we observed that dhS1P mediated the expansion of the same CD19+ CD45R *B220*+ cellular population from isolated hematopoietic progenitors (Figure 7C). We separately performed lineage tracing analysis to confirmed that this population is not of myeloid origin (Supporting Information Figure S6), and this suggested that the perceived expansion of B-cells from isolated immature myeloid cells was simply due to the presence of a "contaminating" progenitor.

Collectively, these results showed that dhS1P, a product of PhotoImmunoNanoTherapy-stimulated SphK activity, can negatively regulate immature myeloid cells that are expanded as part of the tumor-associated pro-inflammatory milieu, which may indirectly promote the expansion of other lymphoid-origin cells. We further isolated these lymphoid-origin cells, which bear the surface characteristics of B-cells, and adoptively transferred them into breast cancer and pancreatic cancer-bearing hosts to achieve therapeutic responses evidenced, respectively, by decreased breast cancer tumor growth or an extension of survival in a model bearing orthotopic pancreatic cancer (Figure 8A, B). Separately, we injected tumor-bearing mice with

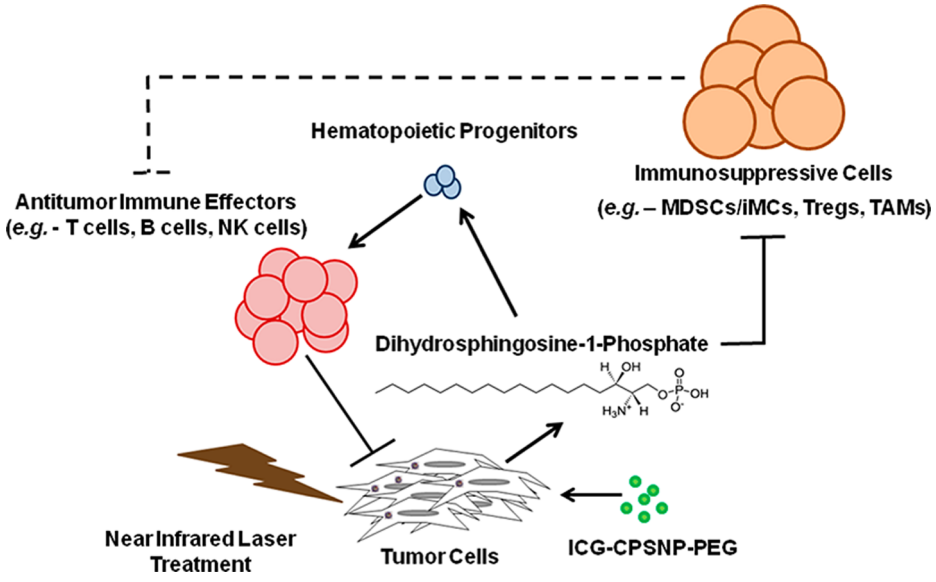

Figure 9. PhotoImmunoNanoTherapy utilizing ICG-CPSNP-PEG exerts an antitumor effect by generating dihydrosphingosine-1-phosphate (dhS1P). Immunosuppressive cells that are often expanded as a function of tumor burden, namely, immature myeloid cells, are ablated by dhS1P. This allows the expansion of immune effector cells from hematopoietic progenitor cells, and this subsequently leads to an antitumor immune response. This mechanism is in addition, and independent from, traditional oxidative-mediated tumor cell death that is a hallmark of photodynamic therapy.

dhS1P and observed a therapeutic effect (Figure 8C). As expected, injection of S1P in this same experiment resulted in augmented tumor growth, owing to the well-defined role of S1P in tumor growth and progression. Altogether, these results showed that dhS1P could mediate the development of an antitumor lymphocyte population. These experiments also offer confirmation that the increase in dhS1P observed in response to PhotoImmunoNanoTherapy is responsible for its immunoregulatory and antitumor effects. It is important to note from these observations that dhS1P-containing therapeutics may exert antitumor efficacy, independent of ICG-CPSNP-based PDT of cancer which generates dhS1P as part of its antitumor mechanism of action.

CONCLUSIONS

In summary, this study demonstrated that PhotoImmunoNanoTherapy is an effective treatment for various solid tumors. Importantly, the mechanism of action involves specific reduction of tumor-linked inflammation and the immature myeloid cells expanded by the tumor inflammatory milieu (Figure 9). More, the antitumor efficacy of PhotoImmunoNanoTherapy was directly attributed to SphK2 and its production of S1P and/or dhS1P, which have the potential to exert epigenetic regulation of cellular stress and inflammatory genetic programs. This study further showed that dhS1P, but not S1P, could specifically abrogate myeloid lineage cells, thereby allowing the expansion of antitumor lymphocytes (Figure 9). Novel therapies are urgently needed to better treat aggressive cancers, as well as to diminish inflammatory and immunosuppressive microenvironments that impede antitumor immunity. This study is significant because it describes (1) PhotoImmunoNanoTherapy as a novel type of PDT, (2) PhotoImmunoNanoTherapy as a therapy that specifically decreases inflammation-expanded immature myeloid cells, (3) a role for SphK2 and the production of S1P and/or dhS1P in the antitumor mechanism of PhotoImmunoNanoTherapy, and (4) a clear and profound role for dhS1P as an immunomodulatory and antitumor bioactive sphingolipid. Therapies that directly or indirectly utilize SphK2-mediated dhS1P production, such as PhotoImmunoNanoTherapy, hold the potential to be revolutionary treatments for cancers with inflammatory and immunosuppressive phenotypes.

MATERIALS AND METHODS

Reagents. Cell culture medium was purchased from Mediatech (Manassas, VA). FBS was obtained from Gemini Bio-Products (West Sacramento, CA), and other cell culture reagents were from Invitrogen (Carlsbad, CA). Antibodies were from eBiosciences (San Diego, CA), BD Biosciences (San Jose, CA), Miltenyi Biotech (Bergisch Gladbach, Germany), and Santa Cruz Biotechnology (Santa Cruz, CA). Unless specified elsewise, other reagents were from Sigma (St. Louis, MO).

Cell Culture. Human BxPC-3 cells were cultured in RPMI-1640 supplemented with 10% FBS and antibiotic-antimycotic solution. Human MDA-MB-231 cells, human SAOS-2-LM7 cells, murine 410.4 cells, and murine Panc-02 cells were cultured in DMEM supplemented with 10% FBS and antibiotic-antimycotic solution. All cultures were maintained at 37 °C and 5% CO_2.

CPSNP Preparation. PEGylated CPSNPs loaded with ICG were prepared as previously described.[6−13] Briefly, a water-in-oil microemulsion using a cyclohexane/Igepal C-520/water system was

used to self-assemble reverse micelles that served as templates for the size-controlled precipitation and surface functionalization of the nanoparticles. Calcium and phosphate, with metasilicate doping, were used as the matrix materials with entrapment of the ICG achieved by matrix precipitation around the fluorophore molecules confined within a reverse micelle. Citrate functionalization was achieved by specific adsorption, providing carboxylate groups for secondary PEG functionalization. A van der Waals laundering procedure was used to remove spectator ions, amphiphiles, and the hydrophobic phase. 1-Ethyl-3-(3-dimethylaminopropyl)-carbodiimide was used to conjugate methoxy-terminated PEG to the CPSNPs. Lastly, centrifugation was used to further wash and concentrate the CPSNPs.

Animal Trials. All animal procedures were approved by the Pennsylvania State University College of Medicine Institutional Animal Care and Use Committee. Orthotopic pancreatic cancer and subcutaneous breast cancer tumors were established in athymic nude, NOD.CB17-*Prkdc*^{scid}/J, BALB/cJ, or C57BL/6J mice as previously described,[8,9] with minor modifications. All cell lines used in animal and cellular studies, prior to any modification, were originally obtained from the American Type Culture Collection (Manassas, VA). For orthotopic BxPC-3-GFP human pancreatic cancer xenografts, 4−6 week old female athymic mice were fully anesthetized with a mixture of ketamine-HCl (129 mg/kg) and xylazine (4 mg/kg) injected intramuscularly. A small incision was made in the left flank, the peritoneum was dissected, and the pancreas exposed. Using a 27-gauge needle, 2.5×10^6 cells, prepared in 100 μL of Hank's balanced salt solution, were injected into the pancreas. For experimental lung-metastatic osteosarcoma xenografts, 4−6 week old female athymic nude mice were tail-vein-injected with 2.5×10^6 human SAOS-2-LM7 cells. For a subcutaneous MDA-MB-231 human breast cancer model, 1×10^7 cells were prepared in 0.2 mL of normal growth media and injected subcutaneously on each side into 4−6 week old female athymic nude mice. For subcutaneous 410.4 murine breast cancer models, 2.5×10^5 cells were similarly prepared and injected into 7 week old female BALB/cJ or 5 week old female NOD.CB17-*Prkdc*^{scid}/J mice. For a subcutaneous Panc-02 murine pancreatic cancer model, 2×10^6 cells were prepared in 0.2 mL of normal growth media and injected subcutaneously on each side into 7 week old male C57BL/6J mice or alternatively into C57BL/6-Tg(Csf1r-EGFP-NGFR/FKBP1A/TNFRSF6)2Bck/J mice (MaFIA mice). All tumor models were allowed to establish for at least one week prior to experimentation.

For PhotoImmunoNanoTherapy, tumor-bearing mice weighing approximately 20 g received 0.1 mL injections of ICG-CPSNPs diluted approximately 1:10 into PBS (200 nM preinjection concentration of ICG), or controls, followed 24 h later by 12.5 J/cm^2 laser NIR irradiation of the subcutaneous tumors, the pancreas, or the lungs (one injection for the MDA-MB-231 breast cancer model, every third day injections for other subcutaneous cancer models, three weekly injections for the orthotopic pancreatic cancer model, and five weekly injections for the metastatic osteosarcoma model). Survival to predetermined humane end points was monitored for the BxPC-3 and SAOS-2-LM7 studies. Tumor volume measurements were performed for MDA-MB-231, 410.4, and Panc-02 studies. In other studies, mice were sacrificed following NIR laser treatment for tumor or serum analysis.

For studies evaluating knockdown of sphingosine kinase, siRNA-transfected MDA-MB-231 cells treated first in culture with PhotoImmunoNanoTherapy (10 nM ICG-CPSNP-PEG for 60 min, followed by 12.5 J/cm^2 NIR irradiation) were tail-vein-injected into tumor-bearing mice (note, for this trial, the initial tumor sizes were larger to allow for less growth-related variation). Tumor size was monitored by caliper measurement (see Figure 6A for schematic and details).

For adoptive transfer studies, immature myeloid cells were first isolated from the splenocytes of tumor-bearing athymic nude mice by cell sorting for Gr-1+ CD11b+ cells. These isolated cells were treated in culture with 5 μM dhS1P prior to adoptive transfer into MDA-MB-231 breast cancer- or BxPC-3 pancreatic cancer-bearing athymic nude mice. Tumor volume measurements were performed for MDA-MB-231 studies, while survival to predetermined humane end points was monitored for the BxPC-3 studies.

For studies evaluating the specific tumor-modulating effects of phosphorylated bioactive sphingolipids, C57BL/6J mice engrafted with subcutaneous Panc-02 pancreatic cancer tumors were injected every other day with S1P or dhS1P conjugated to a BSA carrier protein (0.1 mL of an initial concentration of 100 μM). Tumor size was monitored by caliper measurement.

Cell Sorting and Flow Cytometry. Splenocytes were harvested from tumor-bearing mice by mechanical disruption in red blood cell lysis buffer. Splenocytes were washed, resuspended in PBS with mouse BD Fc block (1 μg per 1×10^6 splenocytes), and incubated for 15 min at 4 °C. For immature myeloid cell isolation, antibodies targeting Gr-1 (FITC) and CD11b (PE-Cy7) were added. Splenocytes were incubated for 15 min at 4 °C with the respective antibodies (1 μg per 1×10^6 splenocytes). Cell isolation was performed by the Pennsylvania State University College of Medicine Flow Cytometry Core Facility utilizing a Dako Cytomation MoFlo high-performance cell sorter. For flow cytometry, splenocytes were prepared in a similar fashion with antibodies targeting Gr-1 (FITC, or APC-eFluor 780), CD11b (PE-Cy7), CD44 (eFluor 605NC), CD115 (PE), gp91^{phox} (DyLight 649), or LY-6C (PerCP-Cy5.5). Multicolor flow cytometry was performed at the Pennsylvania State University College of Medicine Flow Cytometry Core Facility utilizing a BD Biosciences LSR II special order flow cytometer. BD FACS Diva software was used to analyze results. All antibodies were purchased from eBioscience, BD Biosciences, or Santa Cruz. DyLight conjugations were performed with a conjugation kit from Thermo Fisher.

CFU-GEMM Assay. Isolated immature myeloid cells from the spleens of tumor-bearing athymic nude mice were cultured (5×10^4 cells/mL) in GEMM-supportive complete (mouse) methylcellulose media (R&D Systems, Minneapolis, MN), according to the manufacturer's instructions, with BSA, S1P (5 μM), or dhS1P (5 μM). GEMM colonies were visualized and counted after 3 weeks of culture.

Lipidomics. Lipids were extracted from tumors or serum using a modified Bligh−Dyer extraction. Extracts were subjected to liquid chromatography and electrospray ionization-tandem mass spectroscopy (LC-ESI-MS^3) to detect sphingolipid metabolites, as previously described.[40]

Cytokine Multiplex Assay. An R&D Systems Fluorokine Multi-Analyte Profiling kit was used according to the manufacturer's instructions. Briefly, serum was diluted 1:4 into calibrator diluent RD6-40 and then added to a microplate containing analyte-specific microparticles. A biotin antibody cocktail and streptavidin-PE were added according to the manufacturer's instructions, including wash and incubation steps. Lastly, the mixtures were resuspended in wash buffer and analyzed using a BioRad BioPlex analyzer.

RNA Interference. MDA-MB-231 cells were subcultured and allowed to grow until 50−60% confluent. Then, 200 nM SphK1 (Dharmacon catalog number M-004172-03; accession number NM_021972), SphK2 (Dharmacon catalog number M-004831-00; accession number NM_020126), or nontargeted pools of siRNA (Dharmacon catalog number D-001206-14, pool #2) were transfected with Lipofectamine 2000 according to the manufacturer's instructions. Cells were harvested 24 h post-transfection for animal studies. Alternatively, cells were harvested 48 h post-transfection to verify knockdown by Western blot (Supporting Information Figure S7A).

SphK Overexpression. SphK constructs were generously provided by Jong K. Yun of the Department of Pharmacology at the Pennsylvania State University College of Medicine. Murine SphK1 and SphK2 were cloned, and His-tagged mutants were generated as previously described.[41] Transfection of 410.4 cells with His-tagged SphK-containing plasmids using Lipofectamine 2000 was carried out according to the manufacturer's instructions. Stably expressing clones were selected after culture in media containing 50 μg/mL G418 (neomycin analogue). Following clonal expansion in G418-containing media, stable expression was verified by Western blot (Supporting Information Figure S7B).

Statistics. GraphPad Prism 5.0 software was used to plot graphs as well as to determine significance of results. ANOVA (1-way or 2-way), followed by Bonferroni comparisons, or an unpaired student's *t* test, was used to determine significance between treatment groups. A logrank test was used

to determine significance of survival between treatment groups. All data represent averages ± standard error of the mean.

Conflict of Interest: The authors declare the following competing financial interest(s): The Penn State Research Foundation has licensed CPSNPs to Keystone Nano, Inc. (State College, PA) for commercialization. James H. Adair and Mark Kester serve as CSO and CMO of Keystone Nano, Inc., respectively.

Acknowledgment. The authors would like to thank Nate Scheaffer and Dr. David R. Stanford of the Pennsylvania State College of Medicine flow cytometry core facility for their assistance during the course of this study. This study was funded in part by Children's Miracle Network grants to B.M.B. and T.M.R., the G. Thomas Passananti Endowment Fund of the Department of Pharmacology (M.K.), NIH Grant R01-CA117926 to J.P.S., the Miller Family Faculty Fellowship to J.H.A. and E.I.A., and Keystone Nano, Inc. (State College, PA). The Penn State Research Foundation has licensed CPSNPs to Keystone Nano, Inc. (State College, PA) for commercialization. J.H.A. and M.K. serve as CSO and CMO of Keystone Nano, Inc., respectively.

Supporting Information Available: Figures S1–S7 as described in the text. This material is available free of charge *via* the Internet at http://pubs.acs.org.

REFERENCES AND NOTES

1. Ortel, B.; Shea, C. R.; Calzavara-Pinton, P. Molecular Mechanisms of Photodynamic Therapy. *Front. Biosci.* **2009**, *14*, 4157–4172.
2. Juarranz, A.; Jaen, P.; Sanz-Rodriguez, F.; Cuevas, J.; Gonzalez, S. Photodynamic Therapy of Cancer. Basic Principles and Applications. *Clin. Transl. Oncol.* **2008**, *10*, 148–154.
3. Almeida, R. D.; Manadas, B. J.; Carvalho, A. P.; Duarte, C. B. Intracellular Signaling Mechanisms in Photodynamic Therapy. *Biochim. Biophys. Acta* **2004**, *1704*, 59–86.
4. Wainwright, M. Photodynamic Therapy: The Development of New Photosensitisers. *Anticancer Agents Med. Chem.* **2008**, *8*, 280–291.
5. Chatterjee, D. K.; Fong, L. S.; Zhang, Y. Nanoparticles in Photodynamic Therapy: An Emerging Paradigm. *Adv. Drug Delivery Rev.* **2008**, *60*, 1627–1637.
6. Morgan, T. T.; Muddana, H. S.; Altinoğlu, E. I.; Rouse, S. M.; Tabaković, A.; Tabouillot, T.; Russin, T. J.; Shanmugavelandy, S. S.; Butler, P. J.; Eklund, P. C.; *et al.* Encapsulation of Organic Molecules in Calcium Phosphate Nanocomposite Particles for Intracellular Imaging and Drug Delivery. *Nano Lett.* **2008**, *8*, 4108–4115.
7. Kester, M.; Heakal, Y.; Fox, T.; Sharma, A.; Robertson, G. P.; Morgan, T. T.; Altinoğlu, E. I.; Tabaković, A.; Parette, M. R.; Rouse, S. M.; *et al.* Calcium Phosphate Nanocomposite Particles for *In Vitro* Imaging and Encapsulated Chemotherapeutic Drug Delivery to Cancer Cells. *Nano Lett.* **2008**, *8*, 4116–4121.
8. Altinoğlu, E. I.; Russin, T. J.; Kaiser, J. M.; Barth, B. M.; Eklund, P. C.; Kester, M.; Adair, J. H. Near-Infrared Emitting Fluorophore-Doped Calcium Phosphate Nanoparticles for *In Vivo* Imaging of Human Breast Cancer. *ACS Nano* **2008**, *2*, 2075–2084.
9. Barth, B. M.; Sharma, R.; Altinoğlu, E. I.; Morgan, T. T.; Shanmugavelandy, S. S.; Kaiser, J. M.; McGovern, C.; Matters, G. L.; Smith, J. P.; Kester, M.; *et al.* Bioconjugation of Calcium Phosphosilicate Composite Nanoparticles for Selective Targeting of Human Breast and Pancreatic Cancers *in Vivo*. *ACS Nano* **2010**, *4*, 1279–1287.
10. Muddana, H. S.; Morgan, T. T.; Adair, J. H.; Butler, P. J. Photophysics of Cy3-Encapsulated Calcium Phosphate Nanoparticles. *Nano Lett.* **2009**, *9*, 1559–1566.
11. Barth, B. M.; Altinoğlu, E. I.; Shanmugavelandy, S. S.; Kaiser, J. M.; Crespo-Gonzalez, D.; DiVittore, N. A.; McGovern, C.; Goff, T. M.; Keasey, N. R.; Adair, J. H.; *et al.* Targeted Indocyanine Green-Loaded Calcium Phosphosilicate Nanoparticles for *In Vivo* Photodynamic Therapy of Leukemia. *ACS Nano* **2011**, *5*, 5325–5337.
12. Russin, T. J.; Altinoğlu, E. I.; Adair, J. H.; Eklund, P. C. Measuring the Fluorescent Quantum Efficiency of Indocyanine Green Encapsulated in Nanocomposite Particulates. *J. Phys.: Condens. Matter* **2010**, *22*, 334217.
13. Morgan, T. T.; Goff, T. M.; Adair, J. H. The Colloidal Stability of Fluorescent Calcium Phosphosilicate Nanoparticles: The Effects of Evaporation and Redispersion on Particle Size Distribution. *Nanoscale* **2011**, *3*, 2044–2053.
14. Tacelosky, D. M.; Creecy, A. E.; Shanmugavelandy, S. S.; Smith, J. P.; Claxton, D. F.; Adair, J. H.; Kester, M.; Barth, B. M. Calcium Phosphosilicate Nanoparticles for Imaging and Photodynamic Therapy of Cancer. *Discov. Med.* **2012**, *13*, 275–285.
15. Tabakovic, A.; Kester, M.; Adair, J. H. Calcium Phosphate-Based Composite Nanoparticles in Bioimaging and Therapeutic Delivery Applications. *Wiley Interdiscip. Rev. Nanomed. Nanobiotechnol.* **2012**, *4*, 96–112.
16. Adair, J. H.; Parette, M. P.; Altinoğlu, E. I.; Kester, M. Nanoparticulate Alternatives for Drug Delivery. *ACS Nano* **2010**, *4*, 4967–4970.
17. Altinoğlu, E. I.; Adair, J. H. Calcium Phosphate Nanocomposite Particles: A Safer and More Effective Alternative to Conventional Chemotherapy? *Future Oncol.* **2009**, *5*, 279–281.
18. Altinoğlu, E. I.; Adair, J. H. Near Infrared Imaging with Nanoparticles. *Wiley Interdiscip. Rev. Nanomed. Nanobiotechnol.* **2010**, *2*, 461–477.
19. Desmettre, T.; Devoisselle, J. M.; Mordon, S. Fluorescence Properties and Metabolic Features of Indocyanine Green (ICG) as Related to Angiography. *Surv. Ophthalmol.* **2000**, *45*, 15–27.
20. Separovic, D.; Bielawski, J.; Pierce, J. S.; Merchant, S.; Tarca, A. L.; Ogretmen, B.; Korbelik, M. Increased Tumour Dihydroceramide Production after Photofrin-PDT Alone and Improved Tumour Response after the Combination with the Ceramide Analogue LCL29. Evidence from Mouse Squamous Cell Carcinomas. *Br. J. Cancer* **2009**, *100*, 626–632.
21. Saddoughi, S. A.; Song, P.; Ogretmen, B. Roles of Bioactive Sphingolipids in Cancer Biology and Therapeutics. *Subcell. Biochem.* **2008**, *49*, 413–440.
22. Gouaze-Andersson, V.; Yu, J. Y.; Kreitenberg, A. J.; Bielawska, A.; Giuliano, A. E.; Cabot, M. C. Ceramide and Glucosylceramide Upregulate Expression of the Multidrug Resistance Gene MDR1 in Cancer Cells. *Biochim. Biophys. Acta* **2007**, *1771*, 1407–1417.
23. Ogretmen, B. Sphingolipids in Cancer: Regulation of Pathogenesis and Therapy. *FEBS Lett.* **2006**, *580*, 5467–5476.
24. Hannun, Y. A.; Obeid, L. M. Principles of Bioactive Lipid Signalling: Lessons From Sphingolipids. *Nat. Rev. Mol. Cell Biol.* **2008**, *9*, 139–150.
25. Lahiri, S.; Futerman, A. H. The Metabolism and Function of Sphingolipids and Glycosphingolipids. *Cell. Mol. Life Sci.* **2007**, *64*, 2270–2284.
26. Maceyka, M.; Milstien, S.; Spiegel, S. Sphingosine-1-Phosphate: The Swiss Army Knife of Sphingolipid Signaling. *J. Lipid Res.* **2009**, *50*, S272–S276.
27. Oskeritzian, C. A.; Price, M. M.; Hait, N. C.; Kapitonov, D.; Falanga, Y. T.; Morales, J. K.; Ryan, J. J.; Milstien, S.; Spiegel, S. Essential Roles of Sphingosine-1-Phosphate Receptor 2 in Human Mast Cell Activation, Anaphylaxis, and Pulmonary Edema. *J. Exp. Med.* **2010**, *207*, 465–474.
28. Davis, M. D.; Kehrl, J. H. The Influence of Sphingosine-1-Phosphate Receptor Signaling on Lymphocyte Trafficking: How a Bioactive Lipid Mediator Grew up from an "Immature" Vascular Maturation Factor to a "Mature" Mediator of Lymphocyte Behavior and Function. *Immunol. Res.* **2009**, *43*, 187–197.
29. Rivera, J.; Proia, R. L.; Olivera, A. The Alliance of Sphingosine-1-Phosphate and Its Receptors in Immunity. *Nat. Rev. Immunol.* **2008**, *8*, 753–763.
30. Ostrand-Rosenberg, S.; Sinha, P. Myeloid-Derived Suppressor Cells: Linking Inflammation and Cancer. *J. Immunol.* **2009**, *182*, 4499–4506.

31. Gabrilovich, D. I.; Nagaraj, S. Myeloid-Derived Suppressor Cells as Regulators of the Immune System. *Nat. Rev. Immunol.* **2009**, *9*, 162–174.
32. Corzo, C. A.; Cotter, M. J.; Cheng, P.; Cheng, F.; Kusmartsev, S.; Sotomayor, E.; Padhya, T.; McCaffrey, T. V.; McCaffrey, J. C.; Gabrilovich, D. I. Mechanism Regulating Reactive Oxygen Species in Tumor-Induced Myeloid-Derived Suppressor Cells. *J. Immunol.* **2009**, *182*, 5693–5701.
33. Li, H.; Han, Y.; Guo, Q.; Zhang, M.; Cao, X. Cancer-Expanded Myeloid-Derived Suppressor Cells Induce Anergy of NK Cells through Membrane-Bound TGF-β 1. *J. Immunol.* **2009**, *182*, 240–249.
34. Cheng, P.; Corzo, C. A.; Luetteke, N.; Yu, B.; Nagaraj, S.; Bui, M. M.; Ortiz, M.; Nacken, W.; Sorg, C.; Vogl, T.; *et al.* Inhibition of Dendritic Cell Differentiation and Accumulation of Myeloid-Derived Suppressor Cells in Cancer Is Regulated by S100A9 Protein. *J. Exp. Med.* **2008**, *205*, 2235–2249.
35. Youn, J. I.; Nagaraj, S.; Collazo, M.; Gabrilovich, D. I. Subsets of Myeloid-Derived Suppressor Cells in Tumor-Bearing Mice. *J. Immunol.* **2008**, *181*, 5791–5802.
36. Gross, S. A.; Wolfsen, H. C. The Role of Photodynamic Therapy in the Esophagus. *Gastrointest. Endosc. Clin. N. Am.* **2010**, *20*, 35–53.
37. Kotimaki, J. Photodynamic Therapy of Eyelid Basal Cell Carcinoma. *J. Eur. Acad. Dermatol. Venereol.* **2009**, *23*, 1083–1087.
38. Cuvillier, O. Downregulating Sphingosine Kinase-1 for Cancer Therapy. *Expert Opin. Ther. Targets* **2008**, *12*, 1009–1020.
39. Hait, N. C.; Allegood, J.; Maceyka, M.; Strub, G. M.; Harikumar, K. B.; Singh, S. K.; Luo, C.; Marmorstein, R.; Kordula, T.; Milstien, S.; *et al.* Regulation of Histone Acetylation in the Nucleus by Sphingosine-1-Phosphate. *Science* **2009**, *325*, 1254–1257.
40. Wijesinghe, D. S.; Allegood, J. C.; Gentile, L. B.; Fox, T. E.; Kester, M.; Chalfant, C. E. Use of High Performance Liquid Chromatography-Electrospray Ionization-Tandem Mass Spectrometry for the Analysis of Ceramide-1-Phosphate Levels. *J. Lipid Res.* **2010**, *51*, 641–651.
41. Hengst, J. A.; Guilford, J. M.; Fox, T. E.; Wang, X.; Conroy, E. J.; Yun, J. K. Sphingosine Kinase 1 Localized to the Plasma Membrane Lipid Raft Microdomain Overcomes Serum Deprivation Induced Growth Inhibition. *Arch. Biochem. Biophys.* **2009**, *492*, 62–73.